Journal of Materials Chemistry A

Accepted Manuscript

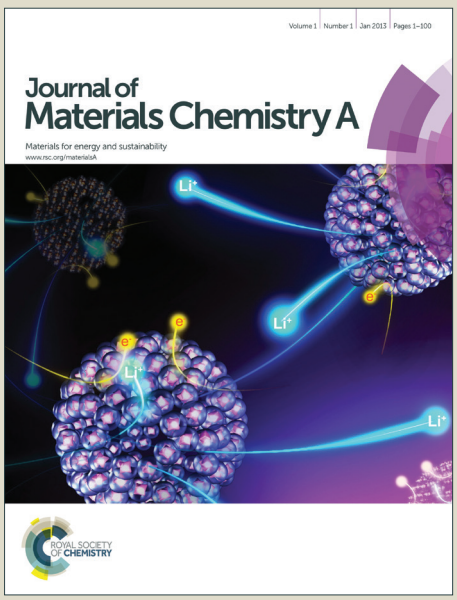

ROYAL SOCIETY OF CHEMISTRY

www.rsc.org/materialsA

A Combined Single Crystal Neutron/X-ray Diffraction and Solid-State Nuclear Magnetic Resonance Study of the Hybrid Perovskites $CH_3NH_3PbX_3$ (X = I, Br and Cl)

Tom Baikie,[1]* Nathan S. Barrow,[2] Yanan Fang,[1] Philip J. Keenan,[3] Peter R. Slater,[3] Ross O. Piltz,[4] Matthias Gutmann,[5] Subodh G. Mhaisalkar[1] and Tim J. White[6]

1 Energy Research Institute @ NTU (ERI@N), Research Technoplaza, Nanyang Technological University, Nanyang Drive, 637553, Singapore.

2 Johnson Matthey Technology Centre, Blount's Court, Sonning Common, Reading, RG4 9NH, UK.

3 School of Chemistry, University of Birmingham, Edgbaston, Birmingham, B15 2TT, UK

4 Bragg Institute, Australian Science and Technology Organisation, Lucas Heights, NSW 2234, Australia.

5 ISIS User Office, Building R3, Rutherford Appleton Laboratory, Chilton, Didcot, OXON, OX11 OQX, United Kingdom.

6 School of Materials Science and Engineering, Nanyang Technological University, Nanyang Avenue, 639798, Singapore.

* Corresponding Author: tbaikie@ntu.edu.sg

Abstract

The ^{1}H and ^{13}C NMR spectra in methylammonium lead halide perovskites, $CH_3NH_3PbX_3$ (X = I, Br and Cl) show that the $CH_3NH_3^+$ units undergo dynamic reorientation, as the organic component tumbles in the perovskite cage. In addition, the differences in the anomalously long relaxation times of the protons associated with the CH_3 and not the NH_3 groups indicate that only the amine end of the $CH_3NH_3^+$ group is interacting with the inorganic network. Using this information, we have refined some single crystal X-ray and neutron diffraction data to probe their unusual structures in more detail. Furthermore, impedance spectroscopy has been used to monitor the high-temperature phase transition of $CH_3NH_3PbI_3$, which confirms a significant increase in conductivity, when it is in its high temperature and higher symmetry structural regime. The optical band-gaps of each halide perovskite were determined using UV-Visible spectroscopy and are consistent with previous reports.

1. Introduction

Photovoltaic devices based on the hybrid perovskite $MAPbX_3$ ($MA = CH_3NH_3^+$; $X = Cl^-$, Br^- and I^-) have drawn attention due to their high solar energy conversion efficiencies[1,2] (20.1%) and potentially economical production using low-temperature (<150°C) solution deposition techniques. An earlier study described the synthesis and structural characterisation of the $MAPbI_3$ perovskite, which confirmed a tetragonal super-structure at room temperature (a = 8.8743(4) Å, c = 12.6708(5) Å) that undergoes phase transitions to cubic ($a \approx 6.3$ Å) and orthorhombic (a = 8.8362(11) Å, b = 12.5804(15) Å, c = 8.5551(10) Å) symmetry at 330K and 161K respectively.[3] This article continues our study of the structural and physical characteristics of $MAPbI_3$ and extends the work to include the $MAPbBr_3$ and $MAPbCl_3$ analogues that have been demonstrated in photovoltaic devices[4, 5] and light emitting diodes.[6]

Establishing the symmetry of the hybrid organic-inorganic perovskite polymorphs is not straightforward. Although $MAPbBr_3$ and $MAPbCl_3$ are reportedly cubic (Pm-3m) at room temperature (25°C),[7] recent work has suggested that the high-temperature phase (T > 57°C) of the $MAPbI_3$ is pseudo-cubic,[8] and possibly tetragonal ($P4mm$) with minor differences in the a and c parameters (a = 6.3115(2) Å, c = 6.3161(2) Å). Moreover, this investigation suggested the room temperature phase was also tetragonal, with $I4cm$ selected over $I4/mcm$ (a = 8.849(2) Å, c = 12.642(2) Å), based on a ferroelectric response observed consistent with non-ohmic behaviour with parabolic I-V dependence. Stoumpos *et al*. deduced that the MA^+ units point along the crystallographic c axis in the tetragonal and 'cubic' regimes. However, this is inconsistent with previous ^2H and ^{14}N NMR findings that found the organic components were dynamically

disordered, with the C-N bond undergoing rapid reorientation in an isotropic potential,[9] whilst in the lower temperature polymorphs (approx. 173K for Cl; 145K for Br and 163K for the I), tumbling of the C-N bond ceases, while reorientation about the C-N axis persists.

To better understand these structures, the synthesis of poly- and single crystalline samples of *MA*PbX_3 (X = Br & Cl) is described and a variable temperature ^{1}H and ^{13}C magic angle spinning nuclear magnetic resonance (MAS-NMR) study of *MA*PbX_3 (X = Cl, Br and I) was undertaken. For *MA*PbI_3 data were collected from room temperature to 80°C to complement our earlier powder X-ray diffraction study.[3] ^{13}C NMR has been used to identify the phase transition in *MA*PbI_3 by detecting the rate of chemical shift change accompanying a change in crystallographic symmetry. ^{1}H NMR also saw a jump in the T_1 relaxation rate of the methyl protons around the phase transition temperature. Simulations of the ^{1}H spinning sideband pattern revealed a reduction in dipolar coupling, confirming the rapid reorientation about the C-N axis in both the room and high temperature regimes. In addition, the high-temperature phase transition of the iodide was examined using impedance spectroscopy, which showed a significant variation in conductivity at the phase transition temperature that is expected to alter the photovoltaic device performance at elevated temperatures. Using the information derived from the SS-NMR study, we have probed the structural and dynamic features of these intriguing materials in more detail, using single crystal X-ray and Laue neutron diffraction techniques, which also signified the dynamic nature of the *MA* groups. Furthermore, UV-Visible spectroscopy has been used to extract the optical band-gaps of each perovskite, which confirmed they absorb strongly across the visible spectrum.

2. Experimental

2.1 Synthesis

Polycrystalline $MAPbX_3$ (X = I, Br and Cl) were prepared by precipitation from a halogenated acid solution using the method of Poglitsch *et. al*.[7] In this procedure, 1.88 g of lead (II) acetate (Chemical Reagents, Sigma) was dissolved in 40 ml concentrated (37 wt%) aqueous HX solution warmed (≈90°C) in a water bath, after which an additional 2 ml of HX solution with 0.45 g of CH_3NH_2 (40% soluble in water, Merck) was introduced. For the chloride analogue it was necessary to add an excess of HCl to prevent the co-precipitation of $PbCl_2$ in agreement with previous work (see also Figure S#).[10] Crystallisation was initiated by cooling the solution from 90ºC to room temperature over 3 hours. The product was washed with acetone and dried overnight at 100 ºC in a vacuum oven. Larger crystals were obtained via slow cooling from 90 to 50°C over 3 days.

2.2 Crystallographic Characterisation

Powder X-ray diffraction: Phase purity was confirmed by powder X-ray diffraction (PXRD) using a Bruker D8 Advance diffractometer (Bragg-Brentano geometry) equipped with a Cu $K\alpha$ X-ray tube operated at 40 kV and 40 mA. The patterns were accumulated using a step size of 0.02° and a dwell time-per-step of 4s. Samples were mounted in a top-loaded trough, which was rotated during data collection. Under these conditions, the intensity of the strongest reflection

was approximately 100000 counts. Pawley fitting of the X-ray data was carried out from 10-140° 2θ using *TOPAS V4.1*.[11]

Single crystal X-ray diffraction: Data were collected for the *MA*PbI_3 at 70°C using an Agilent Supernova diffractometer (Mo *Kα*, λ=0.71073Å) fitted with an Atlas detector, using Mo radiation over an angular range of 3°≤θ≤33°. As noted in previous work,[8] it was preferable to allow the crystal of *MA*PbI_3 to equilibriate for at least one hour after the phase transition to obtain a higher quality data set. This was indicated by the improved R_{Int} values and suggests the material displays a diffuse phase transition, as suggested by a previous variable temperature powder X-ray diffraction study.[3] For *MA*PbX_3 (X = Br and Cl) data were collected on a Bruker Smart Apex II single crystal diffractometer (Mo Kα), over an angular range of 3°≤θ≤33°.

Single crystal Laue Neutron diffraction: Single crystal neutron diffraction data were collected on the KOALA Laue diffractometer at the Open Pool Australian Lightwater (OPAL) reactor operated by the Australian Nuclear Science and Technology Organisation (ANSTO). The Laue method uses polychromatic thermal-neutrons coupled with a large solid-angle (8 steradians) cylindrical image-plate detector. The perovskite crystals of approximate dimensions 1.5 × 1.5 × 1.5 mm were mounted on an aluminium pin with silicone grease. The diffraction patterns were indexed and processed using the LaueG software,[12] with the reflections integrated using a 2D version of the σ(*I*)/*I* algorithm of Wilkinson *et al*.[13] and Prince *et al*.[14]. No absorption correction was necessary. The reflections were corrected for wavelength distribution, detector efficiency and other corrections by comparison of equivalent reflections and multiple observations.[15]

Reflections were accepted with wavelengths between 0.85 Å and 1.7 Å as a good compromise between peak intensity and reducing the effects of harmonic overlap.

For both the single-crystal X-ray and neutron data, structural refinements were performed using Jana 2006,[16] which utilises the Superflip structure solution algorithm.[17] VESTA[18] was used for 3D visualization of the difference Fourier maps to allow identification of structural disorder and regions of excess electron/nuclear density (for neutrons it is not strictly a density but a region of nuclear scattering strength).

Scanning electron microscopy (SEM): Secondary electron images of the respective perovskites were collected on a JEOL field emission scanning electron microscope (JSM 7600F) operated at 2.0 – 5.0 kV. The perovskite samples were prepared by drop-casting a solution of CH_3NH_2 and lead acetate that had been dissolved in HX (X = Br & Cl) acid onto plain glass (SiO_2). The samples were subsequently heated at 100°C for 2-3 mins to aid the formation of the respective perovskites and to dry the sample.

2.3 Diffuse UV-Vis Spectroscopy

The optical diffuse reflectance spectra of $MAPbX_3$ (X = Cl, Br and I) perovskite powders were measured at room temperature using a UV-Visible-NIR spectrophotometer (Shimadzu UV-3600) with integrating sphere attachment (ISR-3100) operating in the 300-1500 nm region. Highly refined barium sulfate powder (Wako, pure) was used as a reflectance standard.

2.4 Solid-State Nuclear Magnetic Resonance (SS-NMR)

SS-NMR spectra were acquired at a static magnetic field strength of 9.4 T ($\upsilon_0(^1H)$ = 400.16 MHz) on a Bruker Avance III console TopSpin 3.1 software. A wide-bore Bruker 4mm WVT magic angle spinning (MAS) probe was used, with ^1H deuterated adamantane at 1.73 ppm and ^{13}C alanine CH_3 at 20.5 ppm. Powdered samples were packed in zirconia MAS rotors with Macor caps spun using boil-off nitrogen. Experimental parameters for each dataset are given in Table S1 of the supplementary details section.

2.5 Impedance Spectroscopy

Conductivity measurements were carried out on a rectangular sample with dimensions 5.47 × 3.24 × 1.07 mm. Opposing faces of the pellet were coated with silver paste and silver electrodes attached, and then heated (100 °C for 1 hour) to ensure bonding. Conductivity measurement were performed using a Solartron 1260 impedance analyser in the temperature range of 37 – 90°C, with an applied voltage of 0.1 V, and over a frequency range of 100 Hz to 10 MHz. The impedance spectra at low temperature showed a single incomplete semicircle, attributed to the bulk, with the resistance extracted by the low frequency intercept of this semicircle based on nonlinear least square fitting Z-view.[19] At higher temperatures a low frequency tail was seen in the impedance, which may be related to a surface/interface layer or grain boundary component. All resistivity values reported are from the main (bulk component) semicircle.

3. Results and Discussion

3.1 Synthesis and Preliminary Characterisation

The synthesised *MA*PbX_3 crystals were black (iodide), bright red/orange (bromide) or colourless (chloride). As described previously,[3] the iodide generally forms rhombohexagonal dodecahedral crystals, while the bromide displayed a variety of faceting from lamellar to dodecahedral; with the chloride adopting rhombohedral forms (see Figures 1 & 2). The same habits were found for smaller crystals observed by scanning electron microscopy (inset - Figures 1 & 2).

Powder X-ray diffraction confirmed the perovskites to be single-phase (Figures 1, 2 & S1). In our previous report,[3] variable temperature powder X-ray diffraction found the iodide exists as a tetragonal supercell at room temperature, which transformed to cubic (or pseudo-cubic/tetragonal)[8] symmetry at 330K. The bromide and chloride phases reportedly adopt cubic symmetry at room temperature[7] and Figures 1 & 2 shows Pawley fits to the diffraction data assuming cubic symmetry in the space group *Pm*-3*m*. This procedure yielded the lattice parameters $a = 5.93129(4)$ Å and $a = 5.68415(6)$ Å for the bromide and chloride respectively. Recent work on *MA*PbI_3 found the high temperature 'cubic' phase to be metrically tetragonal with small differences in the *a* and *c* parameters.[8] Similarly, our previously reported variable temperature powder X-ray diffraction study of *MA*PbI_3 did not show a complete convergence of the *a* and *c* parameters in the high temperature regime,[3] although the resolution did not show clear asymmetry indicative of lower symmetry. For the bromide and chloride phases the difference plot from the Pawley fits appear consistent with the reported cubic symmetry but there

are some subtle differences between the observed and calculated patterns. A future high resolution X-ray synchrotron diffraction study may remove this ambiguity.

A comparison of the UV-Visible spectra found strong absorptions at 412nm, 544nm and 773nm for the Cl, Br and I perovskites respectively (Figure 3), and were used to calculate the optical absorption coefficient (α) according to the Kubelka-Munk equation, $F(R) = \alpha = (1 - R)^2/(2R)$, where R is the reflectance (%). In this manner, optical band gaps for the perovskites were determined to be 1.51, 2.22 and 2.94eV for the iodide, bromide and chloride respectively (Figure 4). In addition, previous work has shown that for these hybrid perovskites, band-gap tuning is possible by mixing the halides. For example, Kitazawa *et al.*[20] found in thin films of $MAPbBr_{3-x}Cl_x$ that the exciton band shifted systematically towards the blue region with increasing Cl content (this work determined the band-gap for the Br and Cl containing analogues to be 2.35 eV and 3.11 eV respectively). More recently, for the $MAPbI_{3-x}Br_x$ series,[4, 21] fabricated as solid-state sensitised photovoltaic devices, a systematic shift of the absorption band edge to shorter wavelength with increasing Br (band gap varying from 1.5eV for the pure iodine containing material to approximately 2.35eV for the bromide was found). In addition, although the substitution of I for Br resulted in reduced power conversion efficiencies (PCE), the materials were less moisture sensitive and the devices produced higher open-circuit voltages (V_{OC}).

3.2 Solid State NMR

^1H MAS NMR

The ^{1}H spectra for each of the perovskites contained two clear peaks with equal populations corresponding to CH_3 and NH_3 environments (Figure 5). Overall, the methylammonium ions appeared isolated from additional protons, as moderate MAS (8 kHz) was sufficient to narrow the linewidths. Locally the protons in the CH_3 and NH_3 environments are hopping rapidly causing further line narrowing. Going from the iodide to the chloride the ^{1}H peaks appear to become narrower as most clearly shown for the CH_3 groups (Figure S2). One cause for such line narrowing is the experimental conditions and Figure S3 shows the ^{1}H spectra for the iodide perovskite for different spinning rates. The *MA*PbI_3 and *MA*$PbCl_3$ were collected at 8 kHz with the *MA*$PbBr_3$ collected at 10 kHz, so the latter is artificially narrowed by the faster spinning rate. Nevertheless, the narrower peaks for the chloride compared to the iodide suggests the *MA* groups are tumbling faster in *MA*$PbCl_3$ than in *MA*PbI_3. The extracted FWHM from the ^{1}H spectra are presented in Table S2. This trend is in agreement with measurements of the rotational correlation times of the MA^+ ion using ^{2}H NMR.[22] For *MA*PbI_3, the high temperature phase transition did not significantly alter the FWHM of the peaks.

Saturation recovery experiments measured the T_1 relaxation times of the iodide perovskite (Figure S4). The T_1 relaxation times were around 16s at room temperature for both CH_3 and NH_3 with a plausible mechanism being spin-rotational relaxation.[23] For each temperature, the saturation-recovery curves for both the CH_3 and NH_3 were fitted to exponentials to extract the T_1 relaxation time. As the data could be fitted well by a single exponential, it indicates that there is one dominant relaxation mechanism acting per environment. The T_1 times are shown in Figure 6 and reveals that the T_1 relaxation time lengthened as the temperature increased because the proton hopping speeds up. This is in agreement with Xu *et al.*[10] who reported that the ^{1}H T_1

increased with increasing temperature smoothly through the high temperature phase transition. Curiously, the CH_3 protons but not the NH_3 protons appeared to have anomalously long relaxation times just before the phase transition. The reason for this is unclear and may be related to the nitrogen being heavier, such that the CH_3 end of the ion is more likely to interact with the changing sides of the cage. However, previous work has shown that only the amine groups of the organic components hydrogen bond with halogens of the perovskite cage,[24, 25] so it would be expected that the NH_3 protons have a jump, rather than the CH_3 protons. In addition, the anomalous relaxation times of these protons before the phase transition suggest that the phase transformation is driven by the organic component and not the Pb-I network. Furthermore, previous work on the layered hybrid perovskites has shown that the organic groups order in a tail-to-tail fashion, such that ammonium "heads" hydrogen bond to the halogens in the inorganic sheets.[25] In the 3D perovskites, such a scenario is not feasible and offers a possible explanation as to why the *MA* groups are constantly rotating in an attempt to avoid any unfavourable interactions or to find favourable low energy bonding.

Spectra of the iodide perovskite above and below the high-temperature phase transition are given in Figure S5. Remarkably, little change was seen in the intensity of the spinning side bands as a function of temperature. Spinning sidebands appear in the spectra because of first-order anisotropies (such as chemical shift anisotropy and dipolar coupling) that are not fully removed by magic angle spinning. To investigate the origin of the spinning side bands the spectra were simulated using the SPINEVOLUTION software.[26] The simulated spectra are shown in Figure 7, overlaid with the experimental simulation. With just 1.7ppm chemical shift anisotropy (CSA)

that is typical for a methyl environment, no spinning sidebands appeared. The CSA had to be increased to a physically unlikely 37ppm to reproduce the observed intensity.

As the positions of the protons in a methylammonium ion are known, full homonuclear coupling based on the six proton locations was included in the simulation, with CSA. No sharp peaks were observed without including infinitely fast proton exchange within each CH_3 and NH_3 group – as the hopping averages the dipolar interaction to zero over NMR acquisition timescales. With infinitely fast exchange within each group and dipolar coupling between the CH_3 and NH_3 groups, the simulated sideband intensities were greater than observed experimentally. Adding CSA made this discrepancy worse. With a sensible CSA value (1.7ppm) the simulated spectrum only matched the experimental spectrum when the homonuclear dipolar coupling strength was reduced approximately four-fold. A reduced dipolar coupling can be accounted for by the methylammonium ions undergoing rapid reorientation. This was described previously by Wasylishen *et al.*[22] who noted that an absence of ^{2}H or ^{14}N quadrupole splitting indicated extremely rapid overall reorientation of the C-N axis in a potential of cubic symmetry.

At very short recycle-delay times an additional peak near NH_3 was visible, which can be seen in the 0.32s inset of Figure S6. An overlay plot of all spectra acquired with a recycle delay of 0.32s at temperatures between 30°C to 80°C is shown in Figure S6. Below 52°C this peak was close to that of the NH_3 signal but as the temperature was raised this peak shrunk and an additional peak grew at around 10ppm to 11ppm, which is in the region of hydrogen bonded sites. The fast relaxation and overall small quantity of this site leads us to believe that these are probably related to impurities such as surface absorbed water or parasitic CH_3NH_3I, although no additional

features were observed in the ^{13}C spectra, which would exclude the latter. For *MA*$PbCl_3$, an additional much sharper peak is observed at 7ppm and was observed to relax much faster than the CH_3 and NH_3 peaks. A second spectrum recorded with a short D1 value of 0.2s preferentially enhanced this signal (Figure S7) and several weaker peaks are visible at around 0.2ppm, 1.0ppm and 1.3ppm. The sharpness of these peaks (FWHM) suggests a highly mobile, liquid-like environment and is tentatively attributed to some surface absorbed water.

^{13}C MAS NMR

Spectra of each perovskite are shown in Figure 8. All spectra showed one ^{13}C site, corresponding to CH_3. The small change in ^{13}C chemical shift for the different halides is because the carbon experienced a slight change in electronic environment in each perovskite, caused by the differently sized halide electron densities. Proton decoupling was needed to get a sharp ^{13}C indicating that ^{13}C and ^{1}H were dipolar coupled. However, a cross-polarisation experiment gave only 2/3 of the signal compared to direct acquisition with decoupling. Usually, for non-mobile carbon environments cross-polarisation increases the ^{13}C signal significantly. This evidence of weakened dipolar coupling matches the findings of the proton NMR, that the methylammonium ion is undergoing rapid reorientation.

Upon heating, the iodide perovskite the ^{13}C peak position moved slightly downfield (Figure 9). The phase transition was passed smoothly with no jumps in position or sudden changes in signal strength, and there were no anomalous measurements in contrast to the ^{1}H T_1 times for the CH_3 protons.

A smooth transition was expected, as previous studies have reported no significant influence on the dielectric constant of the materials when going from tetragonal to 'cubic' symmetry.[7] Poglitsch *et al*.[7] also state that the transition from tetragonal to 'cubic' is accompanied by a slight distortion of the PbI_6 octahedra. Thus, the chemical and physical structure around the carbon is largely unaffected by the phase change. In the high temperature phase the ^{13}C peak position continued to move downfield but at a slower rate. This can be more clearly seen in Figure 10 and was a key indicator of this NMR study of a phase change occurring. Studies on related materials such as $N(CH_3)_4CdCl_3$ reported that ^{13}C shifts are smooth over a phase transition.[27]

3.3 Impedance Spectroscopy of the high temperature phase transition of $MAPbI_3$

In our previous report[3] we confirmed using variable temperature powder X-ray diffraction that *MA*PbI_3 undergoes a structural phase transition at 330K (approx. 57°C). To investigate the effect of this phase transition on the materials transport properties we have used impedance spectroscopy. Figure 11 shows the variation in resistivity as a function of temperature and reveals a significant change at approximately 320K, which is consistent with the observed phase transition temperature.[3] Using the linear section of the high temperature data (plot of log σ vs 1/T) the activation energy for conduction is estimated as 0.376 eV (36.24 kJ mol^{-1}). The observed sharp enhancement in the conductivity at the phase transition is reminiscent of superionic phase transitions in solid acid proton conductors such as CsH_2PO_4,[28] and may indicate proton conduction in these hybrid perovskites, albeit at a significantly lower level than in such systems. The observed activation energy is also similar to activation energies for proton

conduction in such solid acid systems, while the SS-NMR studies also indicated significant proton hopping. However, while there may be significant proton motion, we cannot preclude at this present time that the conduction process is not electronic in nature, and so there is a need for more detailed studies to elucidate the exact nature of the conducting species in these systems. Representative impedance spectra are shown in Figure S8.

3.4 Single Crystal X-ray Diffraction

Previous work described that the room temperature tetragonal structure (*I*4/*mcm* or *I*4*cm*) of *MA*PbI_3 generally produced single crystals that are crystallographically twinned, which hindered detailed structural analysis.[3, 8] Therefore, for better comparison, the three perovskite phases were studied in their higher symmetry structural regimes because the crystals reportedly de-twin during the high temperature phase transition.[8] For the *MA*PbI_3 the data were collected at 70°C, which is beyond the reported phase transition temperature of 57°C, with the data for the bromide and chloride analogues collected at room temperature (25°C).

For the iodide, the automated data processing and indexing procedures contained within the CrysAlisPro software resulted in a convergence to a cubic cell with a = 6.3286(2) Å. However, as previous work has suggested an alternative lower symmetry structure, a manual indexing routine was also performed. This procedure yielded two distinct cells in which 100% of the observed reflections could be indexed in both. The first was a tetragonal-related cell similar to that reported by Stoumpos *et al*.[8] with a = 6.3178(5) Å, b = 6.3181(5) Å, c = 6.3249(5) Å, α = 90.036(6)°, β = 90.007(6)° and γ = 90.040(6)°, and the second, a hexagonal cell with lattice

constants a = 8.9426(5) Å, b = 8.9428(6) Å, c = 10.9465(4) Å, α = 90.009(4)°, β = 90.007(4)° and γ = 120.000(6)° (the equivalent rhombohedral cell is a = 6.3222(4) Å α = β = γ = 90.021(4)°). When such ambiguity arises, the general convention is to select the cell with the higher symmetry, which in this case would be the hexagonal/rhombohedral cell. A transformation from *I*4/*mcm* to a rhombohedral cell would require a first-order phase transition because the system would be going from a material with a unique 4-fold symmetry (with no 3-fold axes) to one with a unique 3-fold (and no 4-fold axes). Previous calorimetry studies have shown that the high temperature phase transition for *MA*PbI_3 is of the first-order (but close to second order),[9] nevertheless, for comparison, structural refinements were carried out in both symmetry types. For the *MA*$PbBr_3$ and *MA*$PbCl_3$ only cubic symmetry was suggested even from a manually indexing routine, however, both of these materials are much further away from their transition temperatures to their higher symmetry structures, so any subtle differences in lattice parameters will be more difficult to detect at room temperature. A future low/variable temperature, high resolution synchrotron powder X-ray diffraction study is planned to investigate the variation in lattice parameters for these systems in more detail.

For *MA*PbI_3 the refinement in tetragonal symmetry was performed in the space group *P*4*mm* as reported previously,[8] with the refinements in hexagonal symmetry conducted in both *R*-3*m* and *R*3*m,* with the latter in analogy to the reported symmetry for the room temperature structure of $CsGeI_3$.[29] The reflection conditions were consistent with each space group however *R*3*m* was investigated based on the ferroelectric response reported by Chung *et al*.[8], however it should be noted that this observation is in contrast with previous studies where no clear ferroelectric properties were observed.[30, 31] In addition, a more recent atomic force microscopy work showed

a piezoelectric effect for *MA*PbI_3.[31] The refined atomic positions, anisotropic atomic displacement parameters (ADPs) and refinement agreement factors are shown in Table S3 – S7. Although the agreement factors slightly preferred the refinement performed in *R*3*m*, this may be a statistical artefact, as there is no significant deviation between the two structures. In addition, inspection of the difference Fourier maps for both symmetry types reveals a spherical region of electron density consistent with a rotating *MA* group (Figure 12). Furthermore, the anisotropic displacement parameters for the iodine positions in each symmetry type suggest significant axial motion in agreement with previous studies.[8] It is however, unclear whether the rotating *MA* group results in the unusual ADPs for the iodide positions because a similar feature was reported for the related inorganic perovskite phase $CsSnI_3$.[32]

The single crystal X-ray diffraction data for *MA*$PbBr_3$ and *MA*$PbCl_3$ were both refined in the cubic space group *Pm*-3*m*. By just considering the Pb (0,0,0) and halogen positions (0.5,0,0) the different Fourier maps showed regions of electron density consistent with a disordered *MA* group (Figure S9), however, the refinements also showed strong Fourier peaks in close location to the Pb sites, which may be indicative that the materials belong to an alternative symmetry group. Interestingly the regions of electron density for the *MA* group for both the Br and Cl materials show differing shapes, which may be indication that the organic components are spinning differently in each material. Alternatively, the different shape could be an indication that in the chloride the *MA* groups are in a more restricted environment as indicted by the NMR data.

3.5 Single Crystal Laue Neutron Diffraction

It is generally preferable to deuterate protonated samples such as *MA*PbX_3 for neutron diffraction experiments because protons have a large incoherent scattering cross section, which can hinder the data collection and its analysis. In addition, protons have a negative neutron scattering cross section that can cancel out with positively scattering isotopes that co-occupy similar atomic positions, which can lead to ambiguous structural refinements.[33] In the case of the *MA*PbX_3 (X = Cl, Br & I), 50% of the constituent atoms are protons and is thus a challenging system to study using neutrons; however, the detection of hydrogen positions cannot be achieved using X-ray based methods. Nevertheless, a previous single crystal neutron diffraction study of *MA*$PbBr_3$ showed that it was possible to collect sufficient data for analysis from protonated analogues.[34] Furthermore, a powder neutron diffraction study of a related hybrid perovskite, $CD_3ND_3GeCl_3$, showed that the deuterium substitution strongly influenced the phase transition temperatures for this material.[35]

For each sample, the data were indexed in a cubic cell because unlike the single crystal X-ray diffraction data for *MA*PbI_3 analogue, the resolution of the experiment was not sufficient to resolve any subtle differences in the lattice dimensions. In addition, the determination of lattice parameters cannot be achieved directly from the Laue method. Nevertheless, any deviation of cubic symmetry was found to be very subtle in the X-ray work, so it was considered a fair approximation for the present analysis.

Using the structural model derived previously from a combined maximum entropy method/single crystal neutron diffraction study of *MA*$PbBr_3$,[34] the structures for *MA*PbX_3 (X = Cl, Br and I) were successfully refined to yield the parameters listed in Tables S8 – S10, and are in good

agreement with a disordered arrangement of the *MA* groups in each material, where there is essentially a ball of positive nuclear scattering from the C/N, which is surrounded by sphere of negative nuclear scattering from the protons.. Although it was possible to refine the atomic displacements of the C/N and H positions using anisotropic displacement parameters, the ellipsoids formed unusual shapes that essentially filled the available void space, adding further confirmation to the disordered nature of the *MA* groups. A representation of the refined structures with isotropic atomic displacement parameters for the C/N and H sites is shown in Figure 10

It is noted that the reliability indices and the intensity of the Fourier peaks in the difference Fourier maps increased for the bromide and chloride containing analogues respectively. Inspection of the difference Fourier maps revealed that the strongest Fourier peak for both the Br and Cl is located near the Pb site at (0 0 0). This feature is suggestive of a small displacement of the Pb^{2+} ions off their ideal atomic position and may be an indication of ferroelectric-type properties; or alternatively the materials may belong to a different symmetry-type, which in either case warrants further investigation. In addition, the *MA*$PbCl_3$ perovskite is expected to display the highest structural distortion as this phase is known to exhibit incommensuration a low temperatures (173K).[36] Our intention is to study these materials further via a pair distribution function (PDF) study at a synchrotron facility, as this technique will be more sensitive to small atomic displacements and any structural disorder present in these structures. Whilst the refinements in cubic symmetry indicate a fully disordered *MA* group, the suggestion of alternative cell/symmetry for the iodide analogue may suggest that that *MA* groups are tumbling more along a specific crystallographic direction. It may be useful in future work to partially

deuterate these materials to investigate this possibility in more detail and the use of a fixed wavelength neutron source may provide a more definitive answer to the correct choice of lattice constants/space group.

4. Conclusions

The ^{1}H and ^{13}C NMR spectra indicates that in the ambient and high temperature structural regimes the *MA* units do not adopt fixed positions in the perovskite structure and are tumbling within the cages formed by the PbI_6 octahedra. The anomalously long relaxation times of the NH_3 protons, but not those associated with the CH_3 suggest that the only the amine end of the methlyammonium group interacts with the perovskite cage. In addition, the narrower ^{1}H spectra for the chloride compared to the iodide suggest the *MA* groups are tumbling faster in $MAPbCl_3$. Furthermore, these results suggested that the recently proposed structure of the iodide analogue with the $CH_3NH_3^+$ fixed in position may require further evaluation. Impedance spectroscopy confirmed earlier reports where a large reduction in resistivity is observed at the high temperature phase transition, which is expected to alter the device performance at elevated temperatures.

5. Acknowledgements

Funding from the National Research Foundation (NRF), Singapore (CPR Award No. NRF-CRP4-2008-03) and access to the X-ray facilities at the Research Complex, at the Rutherford Appleton Laboratory is also gratefully acknowledged. The authors would like to thank Dr

Fengxia Wei for assistance in collecting the single crystal X-ray diffraction data for the *MA*PbX_3 (X = Br & Cl) perovskites and Dr Jonathan Bradley for assistance with SPINEVOLUTION and collecting the *MA*$PbCl_3$ NMR data.

Figures and Tables

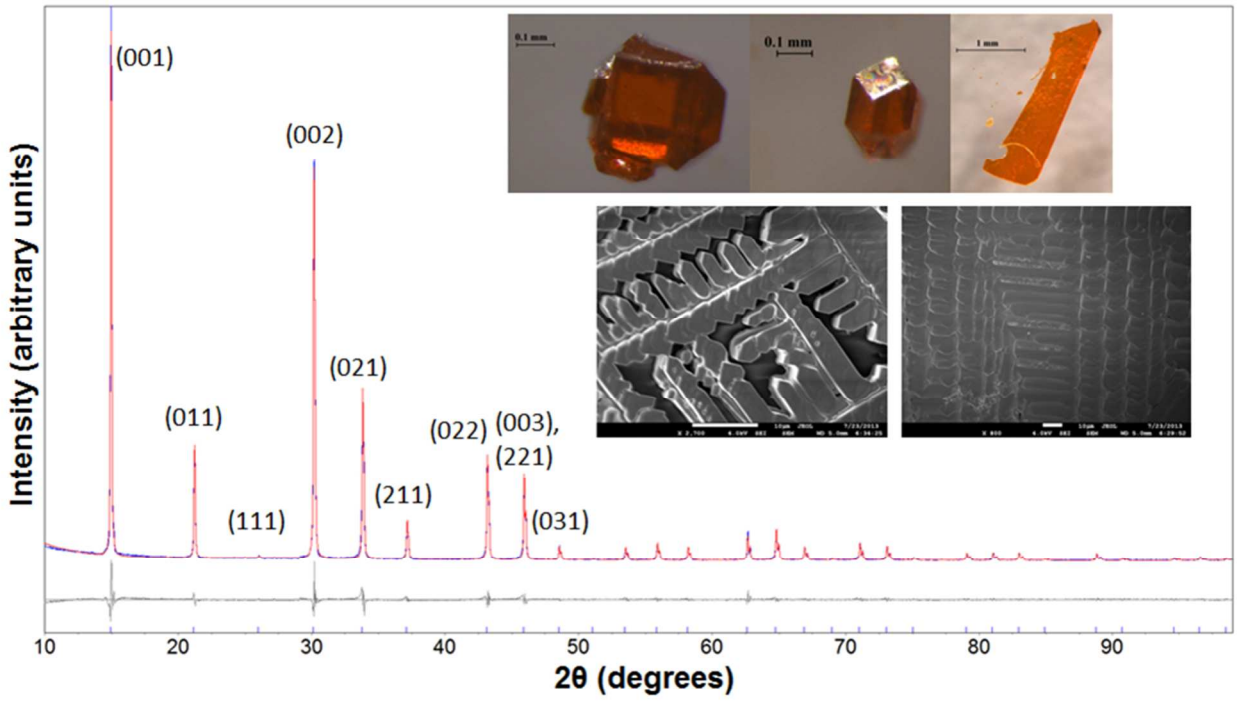

Figure 1. Powder X-ray diffraction pattern of *MA*$PbBr_3$, which has been indexed assuming cubic symmetry (*Pm*-3*m*). Data were collected from a finely ground powdered sample prepared from the solution growth method first described by Poglitsch *et al*.[7] Inset – elongated dodecahedral single crystals and scanning electron microscopy image of *MA*$PbBr_3$ that were drop-casted onto a glass substrate from a solution of CH_3NH_2 and lead acetate in HBr, which was subsequently heated at 100°C for 2-3 mins to dry the sample.

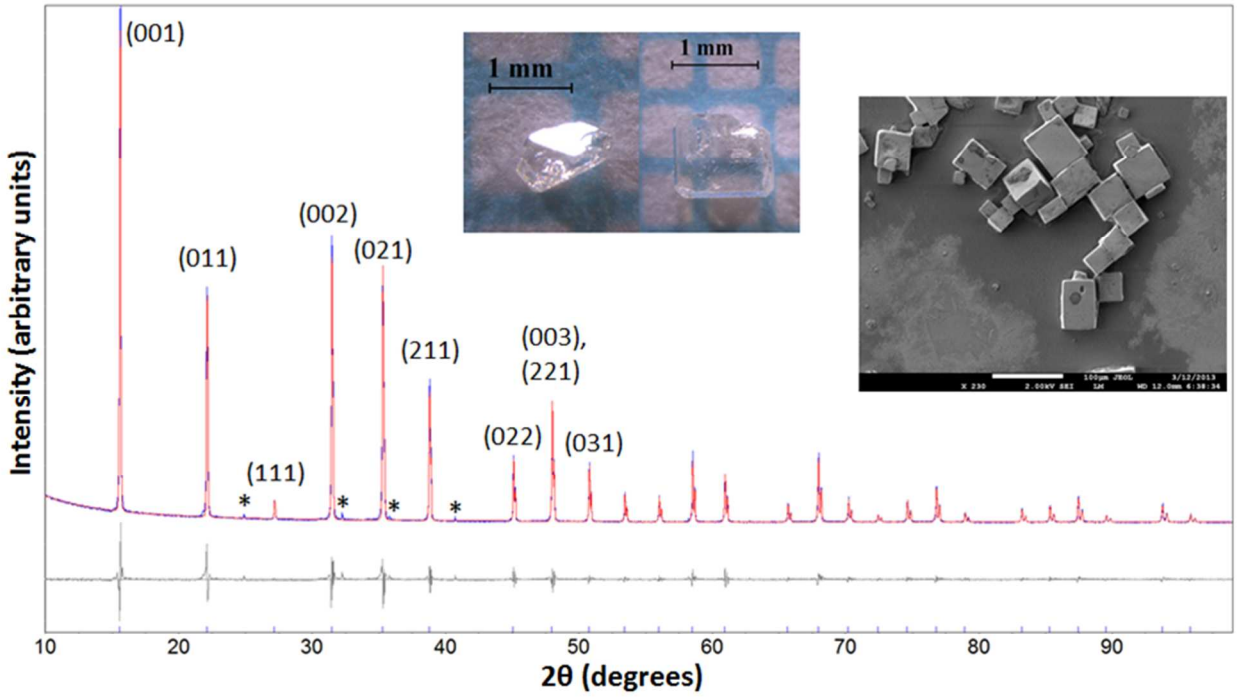

Figure 2. Powder X-ray diffraction pattern of *MA*$PbCl_3$, which has been indexed assuming cubic symmetry (*Pm*-3*m*). Data were collected from a finely ground powdered sample prepared from the solution growth method first described by Poglitsch *et al*.[7] The reflections indicated by * highlight the reflections associated with $PbCl_2$ that are present when HCl is not added in excess. Inset – colourless cubic single crystals and scanning electron microscopy image of *MA*$PbCl_3$ that was drop-casted onto a glass substrate from a solution of CH_3NH_2 and lead acetate in HCl, which was subsequently heated at 100°C for 2-3 mins to dry the sample.

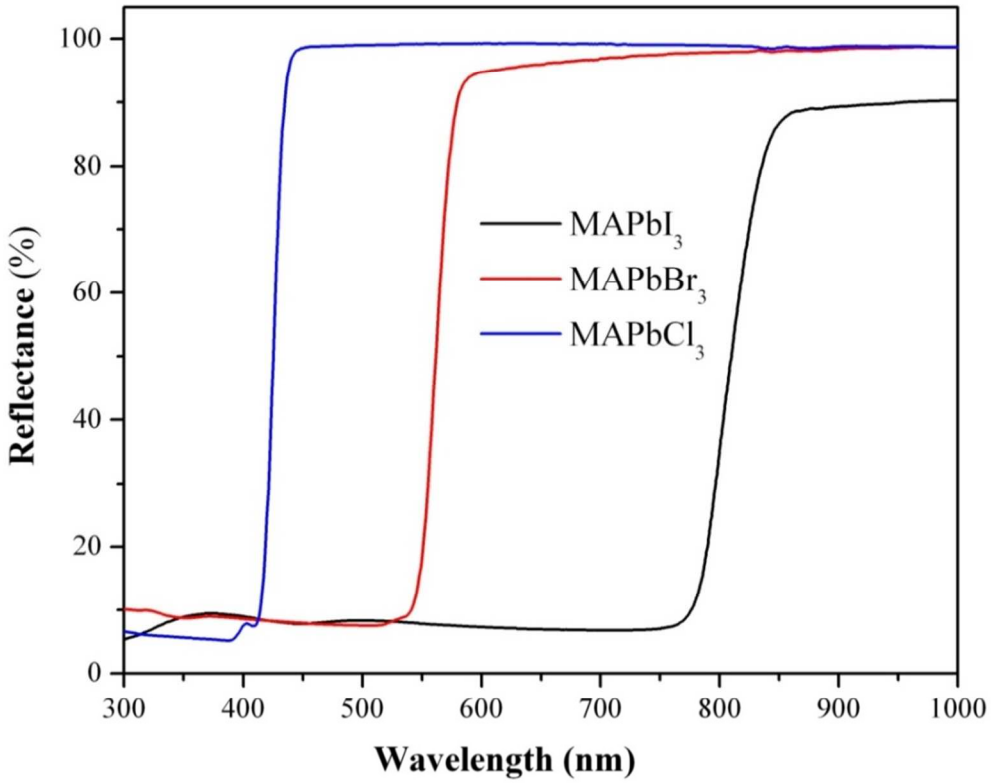

Figure 3. Diffuse reflectance spectra for *MA*PbX_3

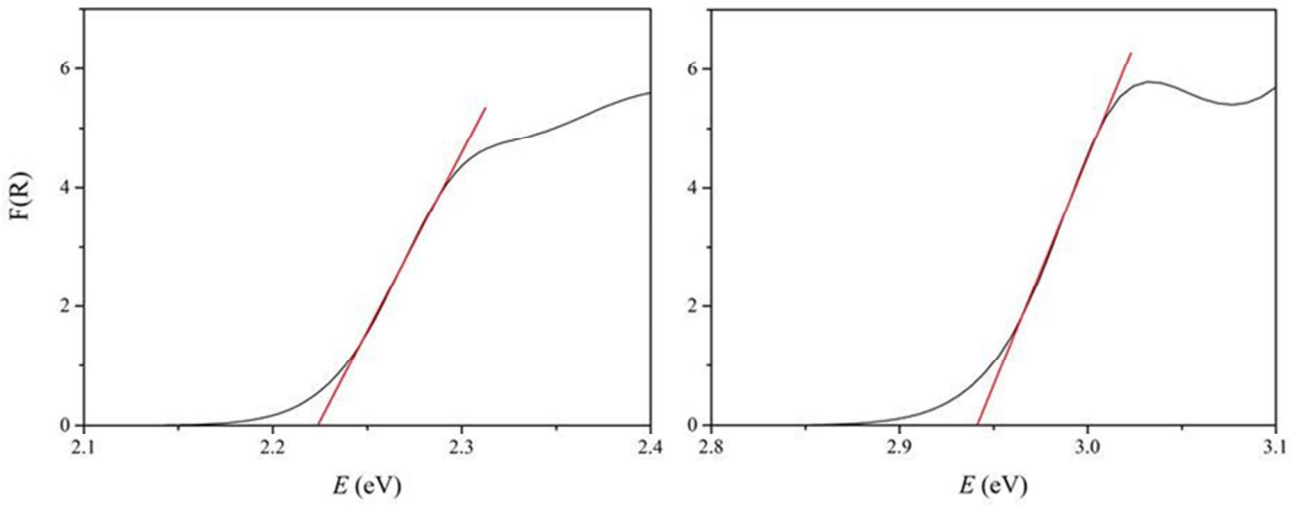

Figure 4. Kubelka-Munk spectra for the *MA*$PbBr_3$ (left) and *MA*$PbCl_3$ (right) revealing optical band-gaps of 2.22 and 2.94 eV respectively.

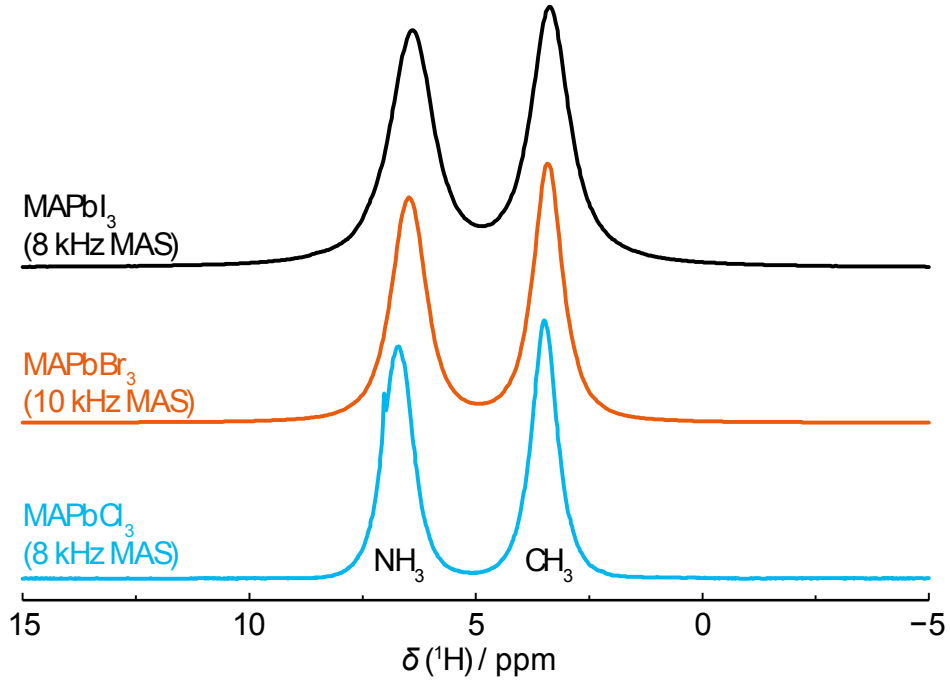

Figure 5. ^{1}H solid-state MAS NMR spectra at room temperature with a recycle delay time of 30s. The sharp peak in the region of the NH_3 proton peak is tentatively attributed to surface absorbed water.

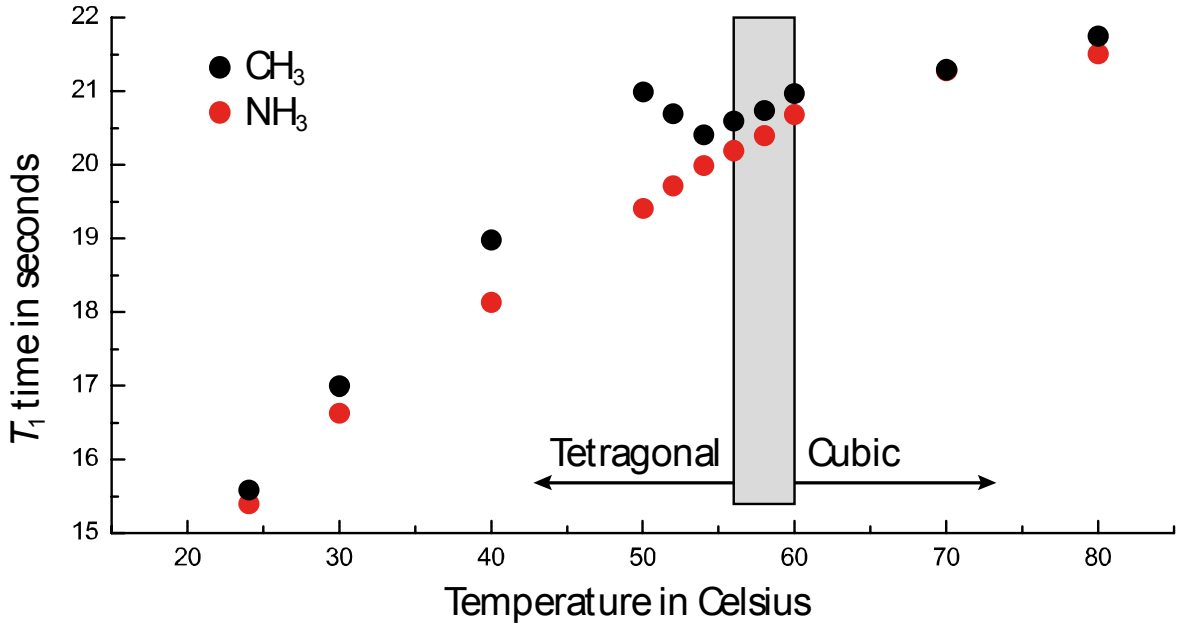

Figure 6. ^{1}H T_1 of $CH_3NH_3PbI_3$ as a function of temperature.

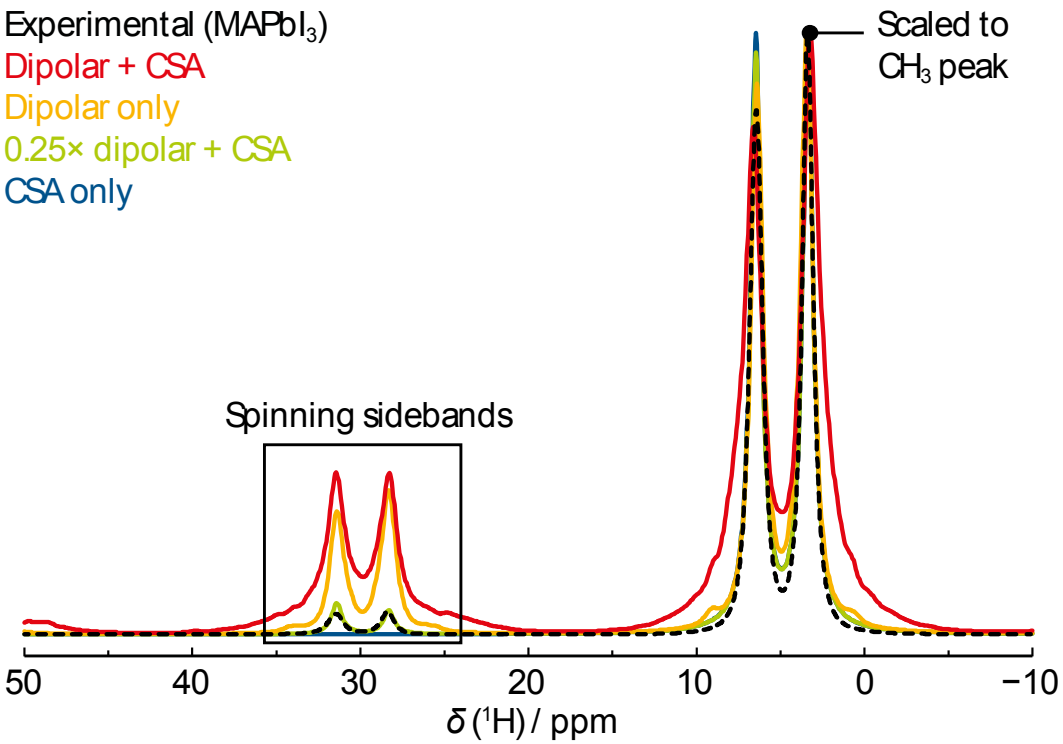

Figure 7. Experimental and simulated ^{1}H solid-state MAS NMR spectra.

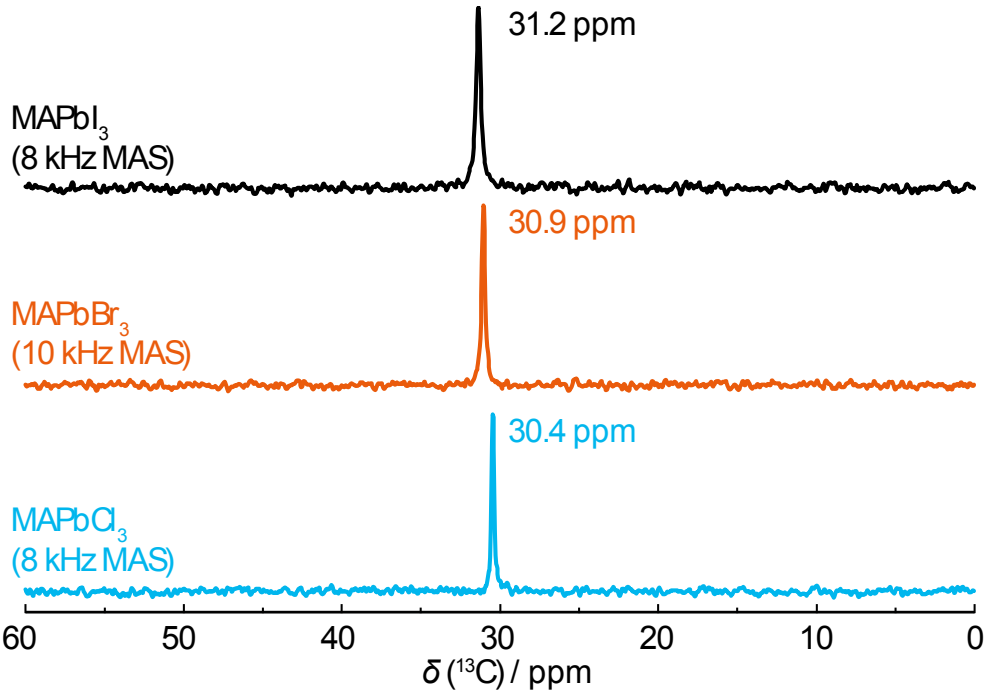

Figure 8. ^{13}C solid-state MAS NMR spectra at room temperature using a direct acquisition with proton decoupling. The ^{13}C spectra for the I, Br and Cl appear at 31.2, 30.9 and 30.4ppm respectively

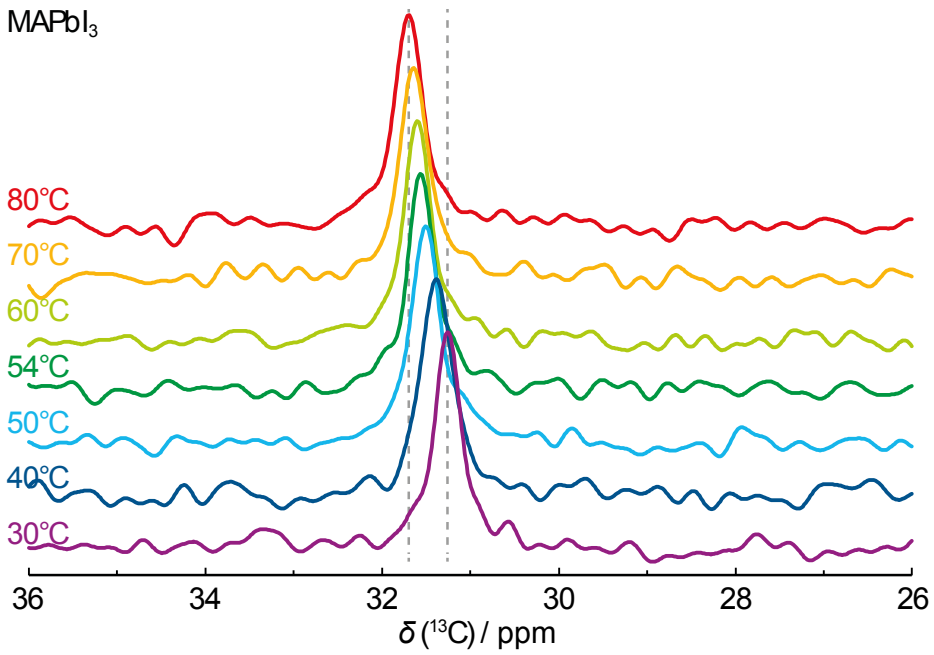

Figure 9. ^{13}C solid-state MAS NMR spectra of $CH_3NH_3PbI_3$ at temperatures between 30°C to 80°C.

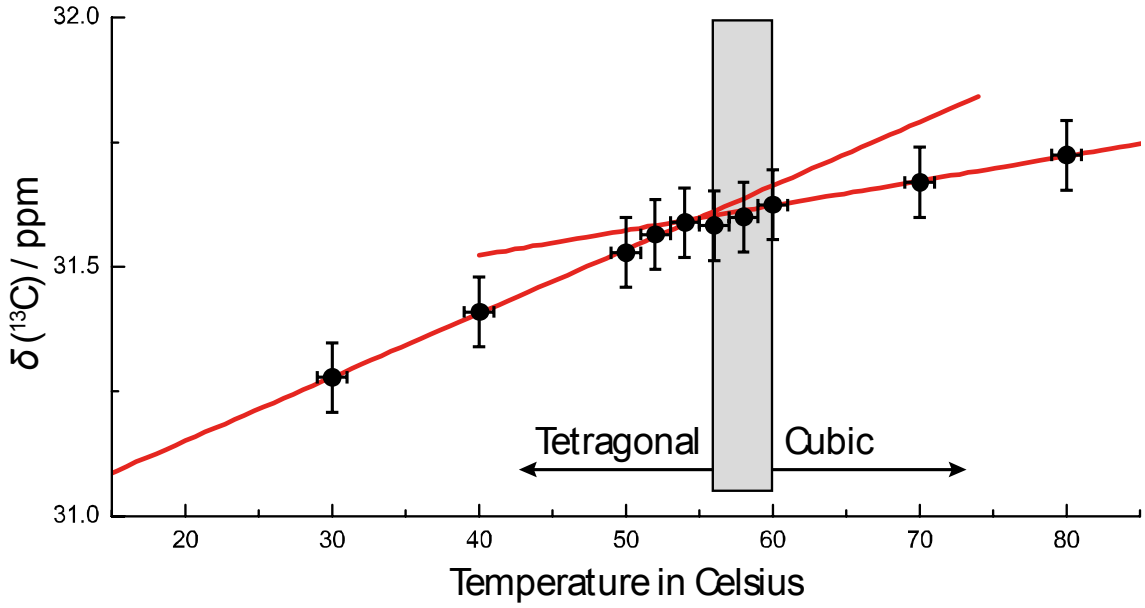

Figure 10. ^{13}C δ_{Iso} of $CH_3NH_3PbI_3$ as a function of temperature. The red lines are linear best fits to the data points above and below the phase transition.

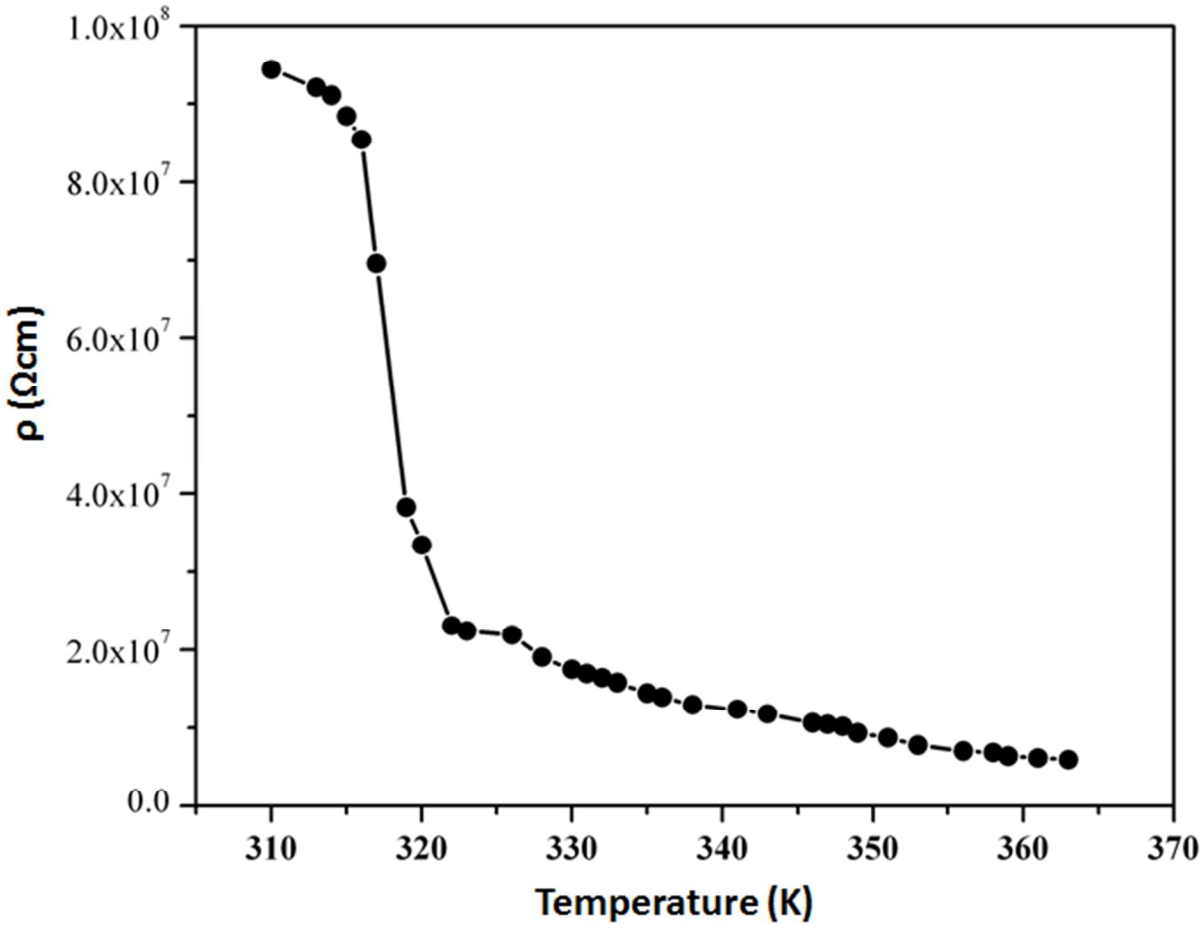

Figure 11. Variation in resistivity for *MA*PbI_3 at the reported high temperature phase transition.

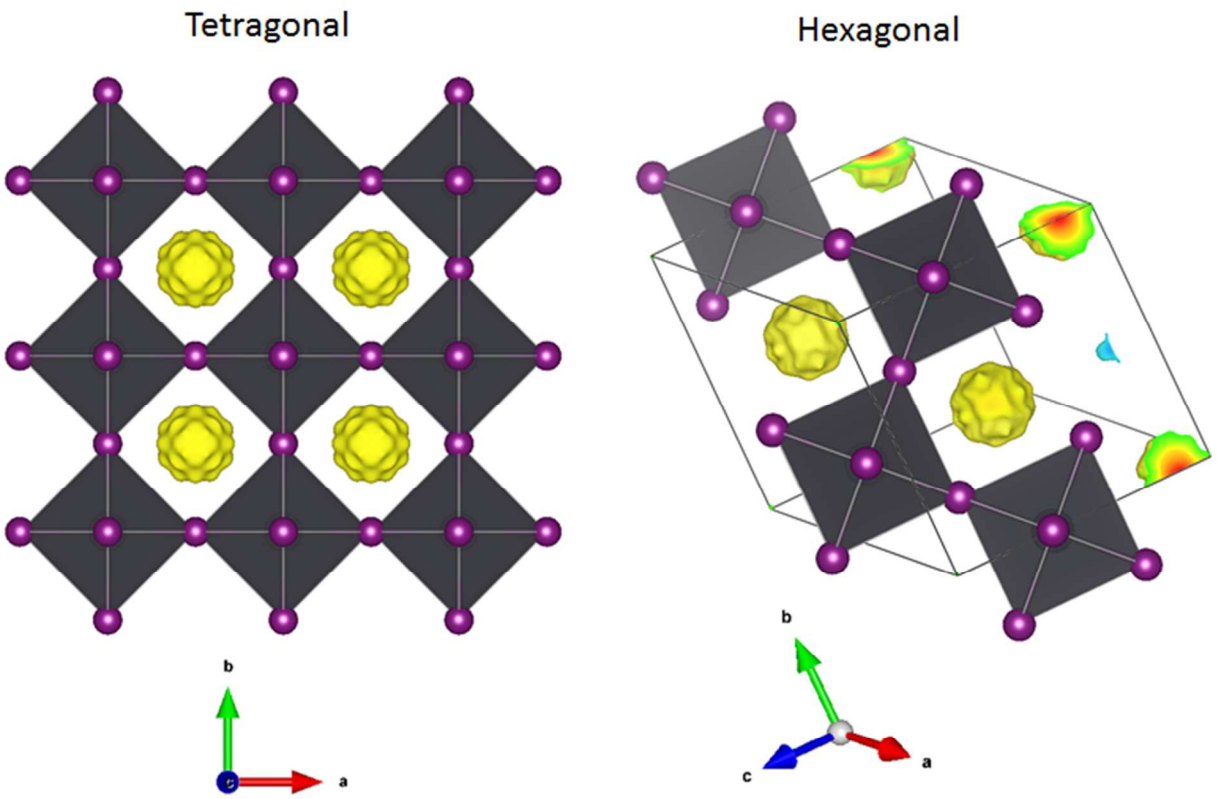

Figure 12. Three dimensional difference Fourier maps for *MA*PbI_3 when refined in both tetragonal (*P*4*mm*) and hexagonal (*R*3*m*) symmetries. The regions of electron density shown in yellow are indicative of a disordered arrangement of the *MA* groups (electron density >1e shown, maximum 2.5e).

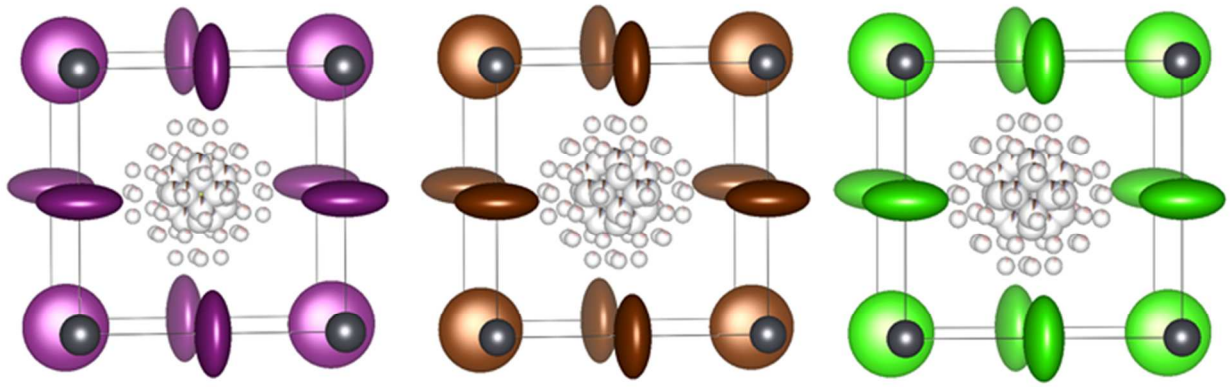

Figure 13. Refined structures of the *MA*PbI_3 (left), *MA*$PbBr_3$ (centre) and *MA*$PbCl_3$ (right) indicating the disordered arrangement of the *MA* groups and the highly anisotropic displacement ellipsoids of the halogen ions (shown with a 90% probability).

References

1. J. Burschka, N. Pellet, S. J. Moon, R. Humphry-Baker, P. Gao, M. K. Nazeeruddin and M. Grätzel, *Nature*, 2013, **499**, 316-319.
2. M. Liu, M. B. Johnston and H. J. Snaith, *Nature*, 2013, **501**, 395-398.
3. T. Baikie, Y. Fang, J. M. Kadro, M. K. Schreyer, F. Wei, S. Mhaisalkar, M. Graetzel and T. J. White, *J. Mater. Chem. A*, 2013, **1**, 5628-5641.
4. J. H. Noh, S. H. Im, J. H. Heo, T. N. Mandal and S. I. Seok, *Nano Letters*, 2013, **13**, 1764-1769.
5. E. Edri, S. Kirmayer, D. Cahen and G. Hodes, *J. Phys. Chem. Lett.*, 2013, **4**, 897-902.
6. Z. K. Tan, R. S. Moghaddam, M. L. Lai, P. Docampo, R. Higler, F. Deschler, M. Price, A. Sadhanala, L. M. Pazos, D. Credgington, F. Hanusch, T. B. Bein, H. J. Snaith and R. H. Friend, *Nature Nanotechnology*, 2014, **9**, 687-692.
7. A. Poglitsch and D. Weber, *J. Chem. Phys.*, 1987, **87**, 6373-6378.
8. C. C. Stoumpos, C. D. Malliakas and M. G. Kanatzidis, *Inorg. Chem.*, 2013, **52**, 9019-9038.
9. N. Onoda-Yamamuro, T. Matsuo and H. Suga, *J. Phys. Chem. Solids*, 1990, **51**, 1383-1395.
10. Q. Xu, T. Eguchi, H. Nakayama, N. Nakamura and M. Kishita, *Z. Naturforsch*, 1991, **46a**, 240-246.
11. Bruker, *Topas Version 4.1*, (2008) Bruker AXS Inc., Madison, Wisconsin, USA.
12. *The Laue G software is available from the author R. O. Piltz*.
13. C. Wilkinson, H. W. Khamis, R. F. D. Stansfield and G. J. McIntyre, *J. Appl. Cryst.*, 1988, **21**, 471-478.
14. E. Prince, C. Wilkinson and G. J. McIntyre, *J. Appl. Cryst.*, 1997, **30**, 133-137.
15. R. O. Piltz, *Acta Cryst.* , 2011, **A67**, C155.
16. V. Petriček, M. Dusek and L. Palatinus, *Jana2006. The crystallographic computing system.*, (2006), Institute of Physics, Praha, Czech Republic.
17. L. Palatinus and G. Chapuis, *J. Appl. Crystallogr.*, 2007, **40**, 786-790.
18. K. Momma and F. Izumi, *J. Appl. Cryst.*, 2008, **41**, 653-658.
19. D. Johnson, (2007) Scibner Associates Inc.
20. N. Kitazawa, Y. Watanabe and Y. Nakamura, *J. Mater. Sci.* , 2002, **37**, 3585-3587.
21. S. A. Kulkani, T. Baikie, P. P. Boix, N. Yantara, N. Mathews and S. Mhaisalkar, *J. Mater. Chem. A*, 2014, **2**, 9221-9225.
22. R. E. Wasylishen, O. Knop and J. B. Macdonald, *Solid state Commun.*, 1985, **56**, 581-582.
23. R. Ikeda and C. A. McDowell, *Chem. Phys. Lett.*, 1972, **14**, 389-392.
24. D. B. Mitzi, *J. Chem. Soc., Dalton Trans.*, 2001, 1-12.
25. D. B. Mitzi, *Prog. Solid State Chem.*, 1999, **48**, 1-121.
26. M. Veshtort and R. G. Griffin, *J. Magn. Reson.*, 2006, **178**, 248-282.
27. A. R. Lim, *Appl. Magn. Reson.*, 2014, **45**, 9-17.
28. S. M. Haile, C. R. I. Chisholm, K. DSasaki, D. A. Boysen and T. Uda, *Faraday Discuss.*, 207, **134**, 17-39.
29. G. Thiele, H. W. Rotter and K. D. Schmidt, *Z. Anorg. Allg. Chem.*, 1987, **545**, 148-156.
30. K. Gesi, *Ferroelectrics*, 1997, **203**, 249.
31. Z. Xiao, Y. Yuan, Y. Shao, Q. Wang, Q. Dong, C. Bi, P. Sharma, A. Gruverman and J. Huang, *Nat. Mater.*, 2014, 10.1038/NMAT4150.

32. I. Chung, J. H. Song, J. Im, J. Androulakis, C. D. Malliakas, H. Li, A. J. Freeman, J. T. Kenney and M. G. Kanatzidis, *J. Am. Chem. Soc.*, 2012, **134**, 8579-8587.
33. T. Baikie, M. H. G. Ng, S. Madhavi, S. S. Pramana, K. Blake, M. Elcombe and T. J. White, *Dalton Trans.*, 2009, 6722-6726.
34. H. Mashiyama, Y. Kawamura, H. Kasano, T. Asahi, Y. Noda and H. Kimura, *Ferroelectrics*, 2007, **348**, 182-186.
35. K. Yamada, K. Mikawa, T. Okuda and K. S. Knight, *J. Chem. Soc., Dalton Trans.*, 2002, 2112-2118.
36. Y. Kawamura and H. Mashiyama, *J. Kor. Phys. Soc*, 1999, **35**, S1437-S1440.

Graphical Abstract

This article describes a variable temperature solid-state NMR and single crystal X-ray/neutron diffraction study of the hybrid perovskites $(CH_3NH_3)PbX_3$ (X = I, Br and Cl).